Josephson junction in a thin film

V. G. Kogan, V. V. Dobrovitski, and J. R. Clem
Ames Laboratory - DOE and Department of Physics and Astronomy, Iowa State University, Ames, Iowa 50011

Yasunori Mawatari
Frontier Technology Division, Electrotechnical Laboratory, 1-1-4 Umezono, Tsukuba, Ibaraki 305-8568, Japan

R. G. Mints
School of Physics and Astronomy, Raymond and Beverly Sackler Faculty of Exact Sciences, Tel Aviv University, Tel Aviv 69978, Israel
(Received 15 November 2000; published 5 March 2001)

The phase difference $\varphi(y)$ for a vortex at a line Josephson junction in a thin film attenuates at large distances as a power law, unlike the case of a bulk junction where it approaches exponentially the constant values at infinities. The field of a Josephson vortex is a superposition of fields of standard Pearl vortices distributed along the junction with the line density $\varphi'(y)/2\pi$. We study the integral equation for $\varphi(y)$ and show that the phase is sensitive to the ratio l/Λ, where $l=\lambda_J^2/\lambda_L$, $\Lambda=2\lambda_L^2/d$, λ_L, and λ_J are the London and Josephson penetration depths, and d is the film thickness. For $l\ll\Lambda$, the vortex ''core'' of the size l is nearly temperature independent, while the phase ''tail'' scales as $\sqrt{l\Lambda}/y^2=\lambda_J\sqrt{2\lambda_L/d}/y^2$; i.e., it diverges as $T\to T_c$. For $l\gg\Lambda$, both the core and the tail have nearly the same characteristic length $\sqrt{l\Lambda}$.

DOI: 10.1103/PhysRevB.63.144501 PACS number(s): 74.50.+r, 74.76.−w

I. INTRODUCTION

Recent interest in Josephson junctions in superconducting films has been driven by experiments probing the properties of grain boundaries and, in particular, the order parameter symmetry.[1–4] In these experiments, the junction plane was normal to the film faces (unlike traditional thin-film large-area Josephson junctions in which the junction plane is parallel to the faces of two films deposited on top of each other). The junctions in fact are lines separating two thin-film banks touching only along the edges. The Josephson vortices at such boundaries are quite different from those at familiar bulk junctions, because the stray magnetic field of a vortex results in an integral equation governing the phase distribution;[5] i.e., the problem becomes *nonlocal* (as opposed to the well studied *local* sine-Gordon equation for junctions between bulk superconductors). The theory of thin-film junctions is just emerging; there have been no attempts made to connect the phase difference at the junction line with the measurable field outside the film. In fact, the data obtained on films are commonly analyzed with the help of bulk formulas; see, e.g., Refs. 1 and 3. One of the motivations for the present work was to fill in this missing link.

In the following section we describe the approach we employ for thin films and demonstrate it by solving the well-known problem of the Pearl vortex.[6] Besides the transparency and some advantages in providing analytic results for the fields in real space, the method can be readily applied to the problem of a thin-film junction. This is done in the next section, where we rederive the integral equation of Mints and Snapiro[5] for the phase difference φ at the junction line, and establish the relation between the phase and the measurable outside magnetic field. The theory contains two characteristic lengths: one is related to physical properties of the junction,

$$l=\frac{c\phi_0}{16\pi^2 j_c\lambda_L^2}=\frac{\lambda_J^2}{\lambda_L}, \tag{1}$$

where λ_J is the Josephson length of a junction made of bulk banks of the same material and with the same critical current density j_c, and λ_L is the London penetration depth of the banks. The other length is that of Pearl which describes the film:

$$\Lambda=\frac{2\lambda_L^2}{d}, \tag{2}$$

with d being the film thickness.

In the next section we study the distribution of the phase difference $\varphi(y)$ along the junction. We show that at large distances the phase approaches the limiting values of 0 or 2π obeying a power law:

$$\varphi(y\to\infty)\approx 2\pi-\frac{2l\Lambda}{y^2}, \tag{3}$$

$$\varphi(y\to-\infty)\approx\frac{2l\Lambda}{y^2}. \tag{4}$$

This constitutes a major difference from the phase distribution in bulk junctions, where $\varphi(y)$ approaches exponentially the limiting values at infinities. We argue that this behavior is prescribed by the stray field outside the film. As is seen from Eqs. (3) and (4), the characteristic length scale for the large-distance phase variation is $\sqrt{l\Lambda}$.

We then consider the asymptotic behavior of the phase in two limiting cases. We show that for $l\ll\Lambda$, the central part of the Josephson vortex (the core) is of a size l which is nearly temperature independent. Since the phase tail has a scale $\sqrt{l\Lambda(T)}$, the vortex structure changes with T. Unlike Joseph-

 ©2001 The American Physical Society

son vortices in bulk junctions, in thin films the phase distribution is not a universal function of coordinates with a unique temperature dependent length scale. Instead this distribution is described by two lengths, the ratio of which is T dependent.

In applications, the length l may reach a micron size, while the Pearl length Λ might not exceed λ_L by much. Hence, the limit $l \gg \Lambda$ is also of interest. We show that in this case the scale of the phase variation in the core is of the same order as in the phase tail; i.e., it is $\sqrt{l\Lambda}$. This is done with the help of a variational technique.

In Section IV we provide examples of $\varphi(y)$ obtained by solving numerically the integral equation in accordance with our asymptotic and variational estimates.

II. THIN FILMS

As was stressed by Pearl,[6] a large contribution to the energy of a vortex in a thin film comes from the stray fields. In fact, the problem of a vortex in a thin film is reduced to that of the field distribution in free space subject to certain boundary conditions at the film surface.[7] Since $\mathrm{curl}\,\mathbf{h} = \mathrm{div}\,\mathbf{h} = 0$ outside, one can introduce a scalar potential for the *outside* field:

$$\mathbf{h} = \nabla\psi, \quad \nabla^2\psi = 0. \tag{5}$$

Consider a thin film situated at $z=0$. The general form of the potential which vanishes at $z \to +\infty$ of the empty upper half-space is

$$\psi(\mathbf{r},z) = \int \frac{d^2\mathbf{k}}{(2\pi)^2}\,\psi(\mathbf{k})\,e^{i\mathbf{k}\cdot\mathbf{r}-kz}, \tag{6}$$

with $\mathbf{k}=(k_x,k_y)$, $\mathbf{r}=(x,y)$, and $k=|\mathbf{k}|$. Here $\psi(\mathbf{k})$ is the two-dimensional (2D) Fourier transform of $\psi(\mathbf{r},z=0)$. In the lower half-space we have to replace z by $-z$ in Eq. (6).

Let the film thickness d be small relative to the bulk penetration depth of the film material λ_L; for simplicity, the latter is assumed isotropic. For a vortex at $\mathbf{r}=0$, the London equations for the film interior read:

$$\mathbf{h} + \frac{4\pi\lambda_L^2}{c}\,\mathrm{curl}\,\mathbf{j} = \phi_0\hat{\mathbf{z}}\,\delta(\mathbf{r}), \tag{7}$$

where $\hat{\mathbf{z}}$ is the unit vector along the vortex axis. Averaging over the thickness d, we obtain

$$h_z + \frac{2\pi\Lambda}{c}\,\mathrm{curl}_z\mathbf{g} = \phi_0\,\delta(\mathbf{r}), \tag{8}$$

where $\mathbf{g}(\mathbf{r})$ is the sheet current density.

Since all derivatives $\partial/\partial z$ are large relative to the tangential $\partial/\partial\mathbf{r}$, the Maxwell equation $\mathrm{curl}\,\mathbf{h} = 4\pi\mathbf{j}/c$ is reduced to conditions relating the sheet current to discontinuities of the tangential field:

$$\frac{4\pi}{c}g_x = h_y^- - h_y^+, \quad \frac{4\pi}{c}g_y = h_x^+ - h_x^-. \tag{9}$$

Here the superscripts $\pm$ stand for the upper and lower faces of the film, $z=\pm d/2$.

If the environments of the upper and lower half-spaces are identical, we have $h_{x,y}^- = -h_{x,y}^+$ and

$$\frac{2\pi}{c}g_x = -h_y^+, \quad \frac{2\pi}{c}g_y = h_x^+. \tag{10}$$

In this case we can consider only the upper half-space and omit the subscript $+$ by the field components.

We substitute Eq. (10) into Eq. (8) and use $\mathrm{div}\,\mathbf{h}=0$:

$$h_z - \Lambda\frac{\partial h_z}{\partial z} = \phi_0\,\delta(\mathbf{r}). \tag{11}$$

Applying the 2D Fourier transform and recalling that $h_z(\mathbf{k}) = -k\psi(\mathbf{k})$ for the upper half-space, we obtain:

$$\psi^P(\mathbf{k}) = -\frac{\phi_0}{k(1+k\Lambda)}; \tag{12}$$

the superscript P is added for convenience of reference to the Pearl vortex. The distribution of the potential ψ everywhere and, in particular, at the film surface follow readily:

$$\begin{aligned}\psi^P(\mathbf{r},z=0) &= -\phi_0\int\frac{d^2\mathbf{k}}{4\pi^2}\,\frac{e^{i\mathbf{k}\cdot\mathbf{r}}}{k(1+k\Lambda)} \\ &= -\frac{\phi_0}{2\pi}\int_0^\infty \frac{dk\,J_0(kr)}{1+k\Lambda} \\ &= \frac{\phi_0}{4\Lambda}\left[Y_0\left(\frac{r}{\Lambda}\right) - \mathbf{H}_0\left(\frac{r}{\Lambda}\right)\right],\end{aligned} \tag{13}$$

where we have used Ref. 11, 6.562.2. Here, $\mathbf{H}_0, Y_0$ are Struve and second-kind Bessel functions; their difference is well studied; see Ref. 8. The field distribution in real space at the film surface is given in Appendix A.

III. THIN-FILM JUNCTION

Let a thin film have a line junction along the y axis.

The London equation everywhere on the film except the junction reads:

$$h_z + \frac{2\pi\Lambda}{c}\,\mathrm{curl}_z\,\mathbf{g} = 0, \quad x \neq 0. \tag{14}$$

At the junction line $x=0$, the current g_y is discontinuous. One can write for the whole x,y plane:

$$h_z + \frac{2\pi\Lambda}{c}\,\mathrm{curl}_z\,\mathbf{g} = f(y)\,\delta(x), \tag{15}$$

where the function $f(y)$ is still to be determined. To this end, integrate Eq. (15) over the area within the contour following the junction banks along $x=\pm 0$ and crossing the junction at y_1 and y_2; see Fig. 1. The magnetic flux through this contour is zero, and we obtain:

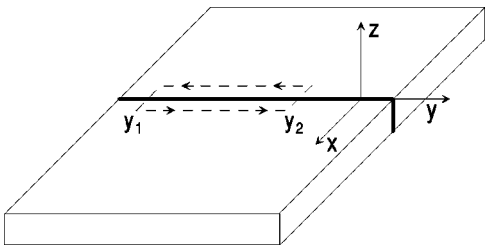

FIG. 1. The junction is shown by a thick solid line. The dashed line shows the contour used to obtain Eq. (16).

$$\frac{2\pi\Lambda}{c}\int_{y_1}^{y_2}[g_y(+0,y)-g_y(-0,y)]\,dy=\int_{y_1}^{y_2}f(y)\,dy \tag{16}$$

for any y_1 and y_2. This gives:

$$\frac{2\pi\Lambda}{c}[g_y(+0,y)-g_y(-0,y)]=f(y). \tag{17}$$

We now use the London relation

$$\mathbf{g}=-\frac{c\phi_0}{4\pi^2\Lambda}\left(\nabla\theta+\frac{2\pi}{\phi_0}\mathbf{A}\right), \tag{18}$$

and the definition of the gauge invariant phase difference

$$\varphi(y)=\theta(-0,y)-\theta(+0,y)-\frac{2\pi}{\phi_0}\int_{-0}^{+0}dx\,A_x(x,y) \tag{19}$$

to obtain

$$\frac{d\varphi}{dy}=\frac{4\pi^2\Lambda}{c\phi_0}[g_y(+0,y)-g_y(-0,y)]. \tag{20}$$

Equations (17) and (20) now yield:

$$f(y)=\frac{\phi_0}{2\pi}\varphi'(y). \tag{21}$$

Thus, we have instead of Eq. (14):

$$h_z+\frac{2\pi\Lambda}{c}\mathrm{curl}_z\mathbf{g}=\frac{\phi_0}{2\pi}\delta(x)\frac{d\varphi}{dy}. \tag{22}$$

This equation serves as the boundary condition for the Laplace problem of the outside field.

As in the Pearl problem, we first rewrite Eq. (22) replacing the sheet currents with tangential fields according to Eq. (10) and using $\mathrm{div}\,\mathbf{h}=0$:

$$h_z-\Lambda\frac{\partial h_z}{\partial z}=\frac{\phi_0}{2\pi}\delta(x)\frac{d\varphi}{dy}, \tag{23}$$

The 2D Fourier transform now yields

$$-(k+k^2\Lambda)\psi(\mathbf{k})=\frac{\phi_0}{2\pi}\tilde{\varphi}'(k_y), \tag{24}$$

where $\tilde{\varphi}'(k_y)$ is the Fourier transform of $d\varphi/dy$. Thus we have:

$$\psi(\mathbf{k})=-\frac{\phi_0\tilde{\varphi}'(k_y)}{2\pi k(1+k\Lambda)}. \tag{25}$$

This gives the outside field distribution in terms of the yet unknown phase difference φ.

One can write Eq. (25) as $\psi(\mathbf{k})=\tilde{\varphi}'(k_y)\psi^P(\mathbf{k})/2\pi$, where $\psi^P(\mathbf{k})$ for the Pearl vortex is given in Eq. (12). This suggests that convolution argument might be useful in relating the field of the junction to that of Pearl vortices. To this end, we take

$$\psi(\mathbf{r},z)=-\int\frac{d^2\mathbf{k}}{(2\pi)^2}\frac{\phi_0\tilde{\varphi}'(k_y)e^{-kz}}{2\pi k(1+k\Lambda)}e^{i\mathbf{k}\cdot\mathbf{r}}, \tag{26}$$

substitute here

$$\tilde{\varphi}'(k_y)=\int_{-\infty}^{\infty}ds\,\varphi'(s)\,e^{-ik_y s}, \tag{27}$$

$$-\frac{\phi_0 e^{-kz}}{k(1+k\Lambda)}=-\int d^2\mathbf{r}'\psi^P(\mathbf{r}',z)e^{-i\mathbf{k}\cdot\mathbf{r}'}, \tag{28}$$

and, after integration over $\mathbf{k}$, obtain

$$\psi(x,y,z)=\int_{-\infty}^{\infty}ds\frac{\varphi'(s)}{2\pi}\psi^P(x,y-s,z). \tag{29}$$

Thus, the field of the Josephson junction is a superposition of fields of Pearl vortices distributed along the junction with the line density $\varphi'(y)/2\pi$.

This remarkable conclusion could have been made on the basis of comparison of Eqs. (8) and (15) which suggests that the Pearl solution for h_z *at the film surface* is the Green's function for $h_z(\mathbf{r},0)$ for arbitrary sources, in our case $\varphi'(y)\delta(x)/2\pi$. The result (29) is more general, since it pertains to all components of the field everywhere outside the film, the surface included. It is worth noting that for bulk junctions, a similar result has been obtained by Gurevich: the field in the junction is a superposition of fields of Abrikosov vortices distributed along the junction with the line density $\varphi'(y)/2\pi$.[9]

To obtain an equation for $\varphi(y)$, we write:

$$\begin{aligned}j_c d\sin\varphi(y)=g_x(0,y)&=-\frac{c}{2\pi}h_y^+(0,y)\\&=-\frac{ic}{2\pi}\int\frac{d^2\mathbf{k}}{4\pi^2}k_y\psi(\mathbf{k})e^{ik_y y}\\&=\frac{c\phi_0}{4\pi^2}\int\frac{d^2\mathbf{k}}{4\pi^2}\frac{\tilde{\varphi}''(k_y)}{k(1+k\Lambda)}e^{ik_y y},\end{aligned} \tag{30}$$

where Eq. (25) has been used. We now substitute the inverse transforms

$$\tilde{\varphi}''(k_y)=\int_{-\infty}^{\infty}dy\,\varphi''(y)\,e^{-ik_y y},$$

$$\frac{4\Lambda}{k(1+k\Lambda)}=\int d^2\mathbf{r}\, e^{-i\mathbf{k}\cdot\mathbf{r}}\left[\mathbf{H}_0\left(\frac{r}{\Lambda}\right)-Y_0\left(\frac{r}{\Lambda}\right)\right] \quad (31)$$

into Eq. (30) and integrate over $\mathbf{k}$ (which is equivalent to utilizing the convolution theorem). We obtain:

$$\sin\varphi(y)=\frac{l}{2}\int_{-\infty}^{\infty}ds\,\varphi''(s)\,Q\left(\frac{|y-s|}{\Lambda}\right),$$

$$l=\frac{c\phi_0}{16\pi^2 j_c\lambda_L^2},\quad Q(w)=\mathbf{H}_0(w)-Y_0(w). \quad (32)$$

This integral equation for the phase has been obtained by Mints and Snapiro using a different technique.[5]

Although both $\mathbf{H}_0(w)$ and $Y_0(w)$ oscillate, the kernel $Q(w)$ decreases monotonically. This is seen from the integral representation:[8]

$$Q(w)=\frac{2}{\pi}\int_0^{\infty}dt\,\frac{e^{-wt}}{\sqrt{1+t^2}}. \quad (33)$$

At small arguments, $\mathbf{H}_0\propto w^2$ while $Y_0(w)$ diverges:

$$Q(w\to 0)\approx-\frac{2}{\pi}\left(\ln\frac{w}{2}+\gamma\right), \quad (34)$$

where γ is the Euler constant. For large w, only small values of t contribute to the integral (33), and we obtain:[8]

$$Q(w)\sim 2/\pi w. \quad (35)$$

With better than 9% accuracy, the kernel can be approximated by a simple function:

$$Q(w)\approx\frac{2}{\pi}\ln\frac{w+1}{w}, \quad (36)$$

which gives correct leading-order asymptotics at $w\to 0$ and $w\to\infty$.

Thus, the equation for the phase contains two independent lengths l and Λ. If Λ is chosen as a unit length, the equation acquires the form

$$\sin\varphi(u)=\mu\int_{-\infty}^{\infty}dv\,\varphi''(v)Q(|u-v|), \quad (37)$$

$$\mu=l/2\Lambda, \quad (38)$$

which shows that only the ratio of these lengths is relevant. Hereafter, we use the notation y,s for coordinates in common units, whereas the variables $u=y/\Lambda$, $v=s/\Lambda$ will be kept dimensionless. When needed we will use also various rescaled variables denoting them as ξ,η.

The solution $\varphi(y)$ should satisfy certain conditions at $y\to\pm\infty$. Since the Josephson current $g_x(0,y)\propto\sin\varphi$ should vanish at infinities, we can choose $\varphi(+\infty)=2\pi$ and $\varphi(-\infty)=0$. At large distances

$$\frac{2\pi}{c}g_x(0,y)=-h_y(0,y)\approx-\frac{\phi_0}{2\pi y^2}\operatorname{sign} y, \quad (39)$$

which means that there the vortex flux ϕ_0 is distributed uniformly over the solid angle 2π. We then obtain for $|y|\to\infty$:

$$\sin\varphi=\frac{g_x}{j_c d}\approx-\frac{2l\Lambda}{y^2}\operatorname{sign} y. \quad (40)$$

The relations given in Eqs. (3) and (4) immediately follow. It is worth recalling that in the bulk junctions the phase $\varphi=4\tan^{-1}(e^{y/\lambda_J})$ approaches the limiting values at infinities as $e^{-|y|/\lambda_J}$.

Another relation follows from fluxoid quantization, which states that the total flux crossing the film is ϕ_0. Since the total flux is $\int d^2\mathbf{r}h_z(\mathbf{r})=h_z(\mathbf{k}=0)$ we have

$$-k\psi(\mathbf{k})|_{\mathbf{k}\to 0}=\left.\frac{\phi_0\tilde{\varphi}'(k_y)}{2\pi(1+k\Lambda)}\right|_{\mathbf{k}\to 0}=\phi_0, \quad (41)$$

which implies that as $k_y\to 0$,

$$\tilde{\varphi}'(k_y)=2\pi,\quad \tilde{\varphi}''(k_y)=0. \quad (42)$$

By splitting the integration domain in Eq. (37) into $v<u$ and $v>u$, we rearrange it to the form:

$$\sin\varphi(u)=\mu\int_0^{\infty}dv\,Q(v)[\varphi''(v+u)-\varphi''(v-u)], \quad (43)$$

where it was assumed that $\varphi'(v)$ is an even and $\varphi''(v)$ is an odd function of v. This form shows that $\varphi(0)=\pi$.

In bulk junctions the vortex field h_z at the junction plane is related to the gradient of the phase difference:

$$h_z(0,y)=\frac{\phi_0}{4\pi\lambda_L}\varphi'(y) \quad (44)$$

(the junction thickness is assumed small relative to λ_L). In thin-film junctions this relation does not hold. Instead, we have, combining Eqs. (17), (21), and (10),

$$h_x(+0,y,0)-h_x(-0,y,0)=\frac{\phi_0}{2\pi\Lambda}\varphi'(y). \quad (45)$$

By symmetry $h_x(+0,y,0)=-h_x(-0,y,0)$; therefore,

$$h_x(+0,y,0)=\frac{\phi_0}{4\pi\Lambda}\varphi'(y). \quad (46)$$

In principle, all fields and currents can be calculated with the help of Eq. (25). Since due to the flux quantization $\tilde{\varphi}'(k_y=0)=2\pi$, Eq. (42), the integrals $\int_{-\infty}^{\infty}dy$ can be evaluated without actual knowledge of $\varphi(y)$. In particular, it is easily shown that

$$\int_{-\infty}^{\infty}\psi(x,y,z)\,dy=\int_{-\infty}^{\infty}\psi^P(x,y,z)\,dy, \quad (47)$$

which implies that similar relations hold for $\int_{-\infty}^{\infty}dy$ of the field components.

A. Asymptotic solution for $l/\Lambda \ll 1$

The length l has a remarkable property of being weakly temperature dependent.[10] Indeed, as T approaches T_c, the product $j_c\lambda_L^2$ is constant because $j_c \propto \Delta^2 \propto (T_c - T)$, while $\lambda_L^2 \propto 1/(T_c - T)$. On the other hand, the Pearl length $\Lambda \propto \lambda_L^2 \propto 1/(T_c - T)$ and diverges at T_c. Therefore, as $T \to T_c$, the ratio $l/\Lambda \to 0$. Also, this ratio might be small for sufficiently thin films for any T. Since the exact solution of the integral Eq. (37) is not available, the search of an approximate result in the limit $\mu \to 0$ is well justified.

It is worth noting that similar to the standard (bulk) Josephson junction, the phase φ varies rapidly only near the vortex center at $y=0$ (within the ''Josephson core'') and the change is slow outside this domain. We will see that the domain of rapid change is of size $\sim \mu \ll 1$, whereas in the rest of the junction the phase varies as a power law. This suggests employing an asymptotic procedure utilizing two different length scales.[12]

Within this method, one looks for the solution of the form

$$\varphi = \sum_{n=0} \varphi_n = \sum_{n=0} \mu^n (c_n + t_n), \quad \mu = l/2\Lambda \ll 1, \tag{48}$$

where the functions $c_n(u)$ and $t_n(u)$ approximate the behavior of φ within the *core* and in the *tail*, respectively, and $u = y/\Lambda$. In particular, this implies imposing the correct boundary conditions at $u=0$ only upon functions $c(u)$, whereas the conditions at ∞'s should be obeyed only by contributions $t(u)$. Still, neither should diverge in the domain of the other (thus providing a uniform asymptotic convergence of the so constructed approximation). Besides, all φ_n should have the correct symmetry (φ_n' must be an even and φ_n'' an odd function of u).

We expect the core to occupy a domain of the size μ (or l in common units), an assumption to be confirmed. To find an equation for $c_0(u)$, we introduce ''stretched'' variables

$$\xi = \frac{u}{\mu}, \quad \eta = \frac{v}{\mu}. \tag{49}$$

One can set $t_0(u) \equiv 0$ and obtain:

$$\sin c_0(\xi) = \int_{-\infty}^{\infty} d\eta\, Q(\mu|\xi - \eta|)\, \frac{d^2 c_0}{d\eta^2}. \tag{50}$$

For $\mu \to 0$, we can use the asymptotic form (34) of the kernel for small arguments. Since $c_0''(\eta)$ is odd in η, the constant terms in the kernel (34) yield zero after integration, and we obtain

$$\sin c_0(\xi) = -\frac{2}{\pi} \int_{-\infty}^{\infty} d\eta \ln|\xi - \eta|\, \frac{d^2 c_0}{d\eta^2}. \tag{51}$$

This equation has an exact solution[13,9,5]

$$c_0(\xi) = 2\tan^{-1}(\xi/2) + \pi. \tag{52}$$

Note that by construction, this formula approximates the actual solution in the core; although the boundary conditions at infinities and at zero are satisfied, the asymptotic behavior of $c_0(\xi)$ at large distances, e.g., $c_0(\xi \to -\infty) \sim 1/\xi$, disagrees with requirements (3) and (4). Therefore, we proceed to the next approximation:

$$\varphi = \varphi_0 + \varphi_1 = c_0 + \mu(t_1 + c_1) \tag{53}$$

and substitute this in Eq. (37):

$$\sin c_0 + \varphi_1 \cos c_0 = \mu \int_{-\infty}^{\infty} dv\, \frac{d^2 c_0}{dv^2} Q(|u-v|) + \mu \int_{-\infty}^{\infty} dv\, \frac{d^2 \varphi_1}{dv^2} Q(|u-v|). \tag{54}$$

We now use Eq. (51) to rewrite this as:

$$t_1 \cos c_0 - \mu \int_{-\infty}^{\infty} dv\, \frac{d^2 t_1}{dv^2} Q(|u-v|) = \int_{-\infty}^{\infty} dv\, \frac{d^2 c_0}{dv^2} \left[Q(|u-v|) + \frac{2}{\pi} \ln|u-v| \right], \tag{55}$$

where we took into account that by design $c_1 \ll t_1$ at large distances. In the limit $\mu \to 0$, the integral at the left-hand side contains an extra factor μ and, therefore, can be disregarded, whereas

$$\frac{dc_0}{du} = \left. \frac{4\mu}{4\mu^2 + u^2} \right|_{\mu \to 0} = 2\pi\delta(u). \tag{56}$$

Hence, for $\xi \gg \mu$, where $\cos c_0 = (\xi^2 - 4)/(\xi^2 + 4) \approx 1$, we obtain:

$$t_1 = 2\pi \frac{dQ(|u|)}{d|u|} + \frac{4}{|u|} \operatorname{sign} u. \tag{57}$$

Thus, at this stage of the expansion we have:

$$\varphi = \varphi_0 + \mu t_1 = 2\tan^{-1}\frac{u}{2\mu} + \pi + 2\pi\mu \frac{dQ(|u|)}{du} + \frac{4\mu}{u}. \tag{58}$$

The last term here compensates both the ''wrong'' behavior of $2\tan^{-1}(u/2\mu)$ at large distances and the divergence of $Q'(|u|)$ at $u=0$. One can see that magnetostatics requirements (3) and (4) are now satisfied.

One should note, however, that while having the correct behavior at large distances, $\varphi_0 + \mu t_1$ acquires a finite discontinuity at the origin:

$$(\varphi_0 + \mu t_1)_{u = \pm 0} = \pi \pm 4\mu. \tag{59}$$

This mismatch is proportional to the small parameter μ and, in principle, could be cured by the core contribution c_1. We omit this difficult calculation, because our major goal of establishing the characteristic lengths of the phase variation is already achieved. Near the vortex center we have:

$$\varphi(y \to 0) = \pi + \frac{2y}{l}, \tag{60}$$

whereas at large distances we have confirmed asymptotics (3) and (4). In other words, l is the characteristic length within the core, whereas at large distances the scale is $\sqrt{l\Lambda}$.

B. The case $l/\Lambda \gg 1$

The length $l \propto 1/j_c$ depends on the junction quality and is often large. It may exceed considerably the Pearl length Λ; this is the case in many experimental situations.[3] It is of interest to consider Eq. (37) in the limit $\mu \to \infty$.

Since $\sin\varphi < 1$ at the LHS of Eq. (37), the equation can be satisfied only if $\varphi'' \to 0$, i.e., if φ is nearly linear in u in a broad domain adjacent to $u=0$. In physical terms, this means that the vortex core is likely to be large. Out of the core, φ is close to the limiting values of 0 and 2π at infinities. To ''shrink'' the core domain we introduce new variables:

$$\xi = u/\sqrt{\mu}, \quad \eta = v/\sqrt{\mu}. \tag{61}$$

Equation (37) now takes the form:

$$\sin\varphi(\xi) = \sqrt{\mu}\int_{-\infty}^{\infty} d\eta \frac{d^2\varphi}{d\eta^2} Q(\sqrt{\mu}\,|\xi-\eta|). \tag{62}$$

In the limit $|\xi| \to \infty$, we can replace the kernel $Q(z)$ with the large argument asymptotics (35). As a result, the parameter μ drops off (this is precisely why the scaling factor has been chosen as $1/\sqrt{\mu}$):

$$\sin\varphi_0(\xi) \approx \int_{-\infty}^{\infty} \frac{d\eta\,\varphi_0''(\eta)}{|\xi-\eta|} \approx \frac{1}{|\xi|}\int_{-\infty}^{\infty} d\eta\,\varphi_0''(\eta)\left(1+\frac{\eta}{\xi}+\ldots\right) \approx -\frac{2\pi}{|\xi|\xi}; \tag{63}$$

we have integrated by parts $\eta\varphi_0''$ and used $\varphi_0''(-\eta) = -\varphi_0''(\eta)$. This result coincides with requirements (3) and (4).

The problem of the core structure can be addressed as follows. The functional, minimization of which leads to Eq. (37) for the phase, reads:

$$W\{\varphi\} = \int_{-\infty}^{\infty} du(1-\cos\varphi) + \frac{\mu}{2}\int_{-\infty}^{\infty} du\,\varphi'(u)\int_{-\infty}^{\infty} dv\,\varphi'(v)Q(|u-v|). \tag{64}$$

It is shown in Appendix B that (within a constant factor) W is in fact the total energy consisting of the Josephson, kinetic, and magnetic contributions. We can now choose a set of trial functions $\varphi_0(u)$ containing a variational parameter which we call L_0; the functions should be linear in u at short distances. Substituting these functions in Eq. (64) we find $W(L_0)$ minimization of which gives the best value for L_0 for a given set.

As an example of this procedure we choose

$$\varphi(u) = 2\tan^{-1}(u/L_0) + \pi, \tag{65}$$

which satisfies the boundary conditions at infinities and varies as $\pi + 2u/L_0$ near the origin. After the calculation outlined in Appendix C, we obtain a relation between L_0 and the parameter μ:

$$2\mu = \frac{\pi L_0(1+4L_0^2)}{\pi + 4L_0\ln 2L_0}. \tag{66}$$

It is seen that for $\mu \ll 1$, L_0 must be small, too. Likewise, large μ require $L_0 \gg 1$. The limiting cases are:

$$2\mu = L_0, \quad \mu \ll 1, \tag{67}$$

$$2\mu = \frac{\pi L_0^2}{\ln 2L_0}, \quad \mu \gg 1. \tag{68}$$

IV. NUMERICAL RESULTS

We have solved numerically the integral Eq. (32) by an iterative method. Starting from a certain trial function $\varphi_0(y)$, we obtain the phase difference after $i+1$ iterations as

$$\varphi_{i+1}(y) = \varphi_i(y) + AD\{\varphi_i(y)\}, \tag{69}$$

$$D\{\varphi(y)\} \equiv -\sin\varphi(y) + \frac{l}{2}\int_{-\infty}^{+\infty} ds\,\varphi''(s)Q\left(\frac{|y-s|}{\Lambda}\right), \tag{70}$$

where A is a constant. Equation (37) is equivalent to $D\{\varphi(y)\}=0$. If the constant A is small enough to stabilize the iterative procedure, the $|D\{\varphi_i(y)\}|$ becomes smaller for larger i. The solution $|D\{\varphi_i(y)\}| < \epsilon$ with an arbitrary accuracy $0 < \epsilon \ll 1$ is obtained by iterating the procedure until $|D\{\varphi_i(y)\}|$ becomes less than ϵ.

The open circles of Fig. 2 show the results of numerical solution of Eq. (37) for the phase difference $\varphi(y')$ with $y' = y/\sqrt{l\Lambda}$ and $l/\Lambda = 0.01$. The solid curve is calculated according to the approximation (52). It is worth observing that the approximation is not only good for small y; it is still fairly good for $\sqrt{l\Lambda} < y < 4\sqrt{l\Lambda}$ (see the inset) and deteriorates slowly at large distances. As we will see below, the large distance behavior has little effect on integrated quantities such as the total vortex energy, mainly because the Josephson currents at these distances are exceedingly small.

Figure 3 shows numerical solutions for $l/\Lambda = 0.01, 0.1, 1, 10$, and 100. One sees that the slope $\varphi'(y)$ at $y=0$ is suppressed; i.e., the vortex ''core'' expands with increasing ratio l/Λ.

To illustrate the core expansion with increasing l/Λ we plot in Fig. 4 the slopes $d\varphi/dy'$ at the origin obtained from the numerical (''exact'') solutions (open circles) along with the slopes calculated using Eq. (66) obtained using the variational procedure described above (solid curve). We see that the trial functions (65) reproduce well $\varphi'(0)$ for small $\mu = l/2\Lambda$, as they should because these functions are close to the actual $\varphi(y)$ for this case. It is worth noting, however, that even for large μ the ansatz (65) provides a reasonable estimate for the slope $\varphi'(0)$.

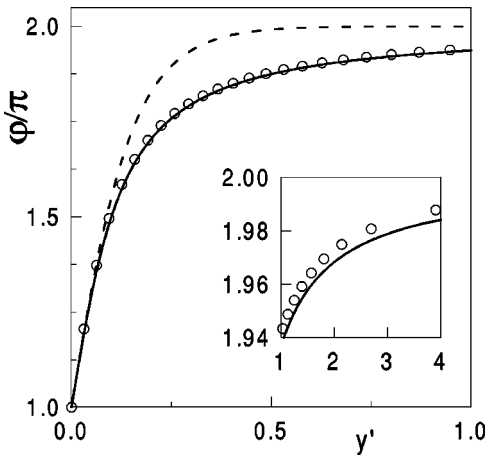

FIG. 2. The phase difference φ versus $y'=y/\sqrt{l\Lambda}$ for $l/\Lambda=0.01$ or $\mu=0.005$. For this and the following plots, $\sqrt{l\Lambda}$ is chosen as unit of length for convenience of comparison. The open circles are obtained by solving numerically the integral Eq. (37). The solid curve is the approximation (52), which reads in terms of y' as $\varphi_0=2\tan^{-1}(y'/\sqrt{2\mu})+\pi$. The inset shows the phase for $y'>1$ or for $y>\sqrt{l\Lambda}$. The dashed curve is the standard bulk soliton $\varphi_b=4\tan^{-1}[\exp(y'/\sqrt{2\mu})]$ which has the same slope at the origin, but approaches the value of 2π exponentially rapidly as $y'\to\infty$.

As is shown in Appendix B, the total energy of a Josephson vortex in a thin film reads:

$$E=\frac{\phi_0^2}{16\pi^3 l}W=\frac{\phi_0^2}{8\pi^2\Lambda}\frac{W(\mu)}{4\pi\mu}. \tag{71}$$

Here, the prefactor $\phi_0^2/8\pi^2\Lambda$ is a natural energy scale because the self-energy of a Pearl vortex is given by this prefactor [multiplied by $\ln(\Lambda/\xi)$ with ξ being the coherence length]. We have calculated E numerically using the trial function (65) with a too slow $1/y$ asymptotics; we tried also the bulk soliton $4\tan^{-1}[\exp(u/L_0)]$, which decays at large distances faster than the needed $1/y^2$. For each trial function,

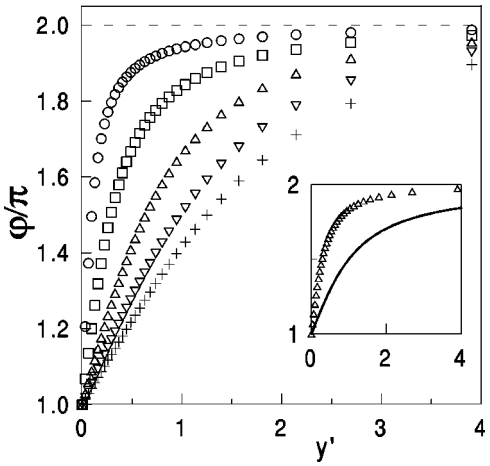

FIG. 3. Numerical solutions $\varphi(y')$, $y'=y/\sqrt{l\Lambda}=u\sqrt{\Lambda/l}$, of Eq. (37) for $l/\Lambda=0.01$ (open circles), 0.1, 1, 10, and 100 (crosses). The inset ($l/\Lambda=1$) shows that the approximation (52), the solid curve, which is good for $l/\Lambda=0.01$ fails for $l/\Lambda=1$.

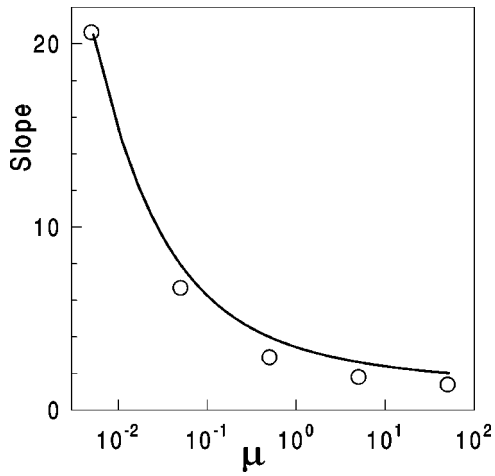

FIG. 4. The slopes $\varphi'(y'=0)$ for the set of $\mu=l/2\Lambda$ shown in Fig. 3 obtained by solving numerically Eq. (37) (open circles). The solid line is obtained with the help of the variational result (66).

we found L_0 which minimizes the energy. Then we evaluated E numerically using the exact kernel Q. Figure 5 shows that these two approximations yield nearly the same energies; the relative difference between them is plotted in the inset and shows that the thin film ansatz yields lower energies for $\mu\ll 1$, whereas the bulk ansatz is better for large μ.

V. SUMMARY

To summarize, we reiterate the following points:

The field associated with a Josephson vortex is a superposition of fields of Pearl vortices distributed along the junction with the line density $\varphi'(y)/2\pi$.

The Josephson vortex in thin films extends to much larger distances than in the bulk due to the $(L_\infty/y)^2$ decay of the

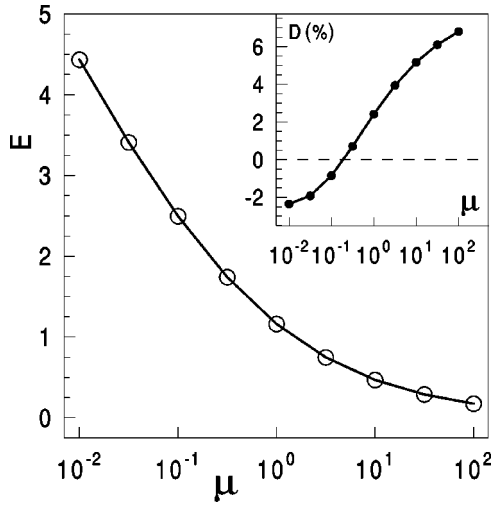

FIG. 5. The energy E of Eq. (71) in units of $\phi_0^2/8\pi^2\Lambda$ as a function of $\mu=l/2\Lambda$ evaluated for the film ansatz $\varphi=2\tan^{-1}(u/L_0)+\pi$ with L_0 chosen to minimize the energy functional (64). The inset shows the relative difference $D=(E-E_b)/E_b$ between E and the energy E_b calculated in the same way with the bulk ansatz $\varphi_b=4\tan^{-1}\exp(u/L_0)$.

phase difference at large distances. This power law is imposed by the magnetostatics of the stray fields outside and as such is the same for any film thickness (as long as $d \ll \lambda_J$ and the z dependence of the phase can be disregarded). The characteristic length L_∞ for the phase attenuation at large distances is

$$L_\infty \approx \sqrt{l\Lambda} \sim \lambda_J \sqrt{\frac{\lambda_L}{d}}. \tag{72}$$

Hence, for moderately thin films ($d \sim \lambda_L$), the length L_∞ is of the order of the bulk Josephson length.

The characteristic length L_0 at small distances (the core size) is l for $l \ll \Lambda$ as is seen from Eq. (52). This is the case in very thin films and for any film thickness close enough to T_c. Thus, for $l \ll \Lambda$, the Josephson vortex is characterized by two lengths, $L_\infty = \sqrt{l\Lambda}$ at large distances and $L_0 = l$ at short ones. These two lengths have different T dependencies, and therefore the vortex structure changes with temperature. Hence, the situation in films is distinctly different from that in bulk junctions, where the structure is universal for all T and is characterized by a single length $\lambda_J(T)$.

For $l \gg \Lambda$, the characteristic length at all distances is of the same order:

$$L_0 \approx L_\infty \approx \sqrt{l\Lambda}. \tag{73}$$

The results obtained in this work for the thin-film limit, $d \ll \lambda_L$, should hold also for thicker films as long as one can disregard the z dependence of the phase. Without going into formal details of the difficult problem of a junction in a slab of finite thickness, we may guess that the z dependence of φ is weak when $d \ll \lambda_J$, since λ_J is the shortest length at which the phase can vary (λ_J is assumed to exceed λ_L). This makes our results applicable to experimental situations as those of Ref. 3 where junctions in YBCO films with $\lambda_L \approx 0.15$ μm and $\lambda_J \sim 1$ μm have been studied.

ACKNOWLEDGMENTS

Ames Laboratory is operated for U.S. DOE by the Iowa State University under Contract No. W-7405-Eng-82. The work of V.G.K. and R.G.M. were supported in part by Grant No. 96-00048 from the United States-Israel Binational Science Foundation (BSF), Jerusalem, Israel. R.G.M. acknowledges hospitality and support of the International Institute of Theoretical and Applied Physics of the Iowa State University. Y.M. is pleased to acknowledge the support of Science and Technology Agency in Japan for his visit to Iowa State University.

APPENDIX A

The component h_z at the film surface is

$$h_z(r,0) = \frac{\phi_0}{2\pi\Lambda}\left\{\frac{1}{r} - \frac{\pi}{2\Lambda}\left[\mathbf{H}_0\left(\frac{r}{\Lambda}\right) - Y_0\left(\frac{r}{\Lambda}\right)\right]\right\}. \tag{A1}$$

We have for $r \ll \Lambda$:

$$h_z(r,0) = \frac{\phi_0}{2\pi\Lambda\, r}\left[1 + \frac{r}{\Lambda}\ln\left(\frac{r}{\Lambda}\right) + \mathcal{O}\left(\frac{r}{\Lambda}\right)\right]. \tag{A2}$$

It is interesting to note that the field in this domain diverges faster than in the bulk vortex for $r \ll \lambda_L$, where $h_z \propto \ln(r/\lambda_L)$. For $r \gg \Lambda$, one can use the asymptotic expansion (12.1.30) of Ref. 8:

$$h_z(r,0) = \frac{\phi_0 \Lambda}{2\pi r^3}\left[1 - \mathcal{O}\left(\frac{\Lambda^2}{r^2}\right)\right]. \tag{A3}$$

The tangential component at the film surface is

$$h_r(r,0) = \frac{\partial\psi}{\partial r} = \frac{\phi_0}{4\pi\Lambda^2}\left[\mathbf{H}_1\left(\frac{r}{\Lambda}\right) - Y_1\left(\frac{r}{\Lambda}\right) - \frac{2}{\pi}\right]. \tag{A4}$$

The asymptotics are readily obtained:

$$h_r(r,0) = \frac{\phi_0}{\pi\Lambda r}\left[1 - \frac{r}{\Lambda} - \frac{r^2}{2\Lambda^2}\ln\frac{r}{2\Lambda} + \mathcal{O}\left(\frac{\Lambda^2}{r^2}\right)\right] \tag{A5}$$

for $r \ll \Lambda$, and

$$h_r(r,0) = \frac{\phi_0}{2\pi r^2}\left[1 - \frac{3\Lambda^2}{r^2} + \mathcal{O}\left(\frac{\Lambda^4}{r^4}\right)\right] \tag{A6}$$

for $r \gg \Lambda$. As expected, the behavior at large distances corresponds to the Coulomb field of a point ''charge'' creating the flux ϕ_0 in a solid angle 2π. Note also the $1/r$ divergence of h_r at $r \to 0$.

APPENDIX B

The Josephson coupling energy is

$$E_J = \frac{\phi_0^2}{16\pi^3 l}\int_{-\infty}^{\infty}\frac{dy}{\Lambda}(1 - \cos\varphi). \tag{B1}$$

The magnetic field energy in the upper half-space is expressed in terms of the potential ψ:

$$\int h^2 \frac{dV}{8\pi} = \int \nabla\cdot(\mathbf{h}\psi)\frac{dV}{8\pi} = -\int \frac{d^2\mathbf{r}}{8\pi} h_z(\mathbf{r},0)\,\psi(\mathbf{r},0)$$

$$= \frac{1}{8\pi}\int \frac{d^2\mathbf{k}}{4\pi^2} k\,\psi(\mathbf{k})\,\psi(-\mathbf{k}). \tag{B2}$$

The total field energy E_F is twice this amount. The kinetic energy E_K of the supercurrents is the integral over the film volume of the quantity $2\pi\lambda_L^2 j^2/c^2 = \pi\Lambda g^2/c^2 d$. Since according to Eqs. (10) $g^2 = c^2(h_x^2 + h_y^2)/4\pi^2$ ($h_{x,y}$ are taken at $z = 0$), we find readily:

$$E_K = \frac{\Lambda}{4\pi}\int \frac{d^2\mathbf{k}}{4\pi^2} k^2\,\psi(\mathbf{k})\,\psi(-\mathbf{k}). \tag{B3}$$

It is now straightforward to show with the help of Eqs. (25), (27), and (31) that the total energy

$$E = E_J + E_F + E_K = \frac{\phi_0^2}{16\pi^3 l} W, \tag{B4}$$

where W is given in Eq. (64).

APPENDIX C

The first integral in Eq. (64) is easily evaluated for the ansatz (65):

$$W_1 = 2\pi L_0. \tag{C1}$$

One can estimate the contribution W_2 of the double integral as follows. Since for the ansatz (65) $\varphi'(u) = 2L_0/(u^2 + L_0^2)$, we have

$$W_2 = 2\mu L_0^2 \int\int \frac{du\, dv\, Q(|u-v|)}{(L_0^2+u^2)(L_0^2+v^2)} = 16\mu L_0^2 \int\int \frac{ds\, dt\, Q(|t|)}{[4L_0^2+(s+t)^2][4L_0^2+(s-t)^2]}. \tag{C2}$$

Here, all integrals are from $-\infty$ to ∞ and we have changed variables: $s = u+v$, $t = u-v$. After integration over s one obtains:

$$W_2 = 8\pi\mu L_0 \int_0^\infty \frac{dt\, Q(t)}{4L_0^2 + t^2}. \tag{C3}$$

Further analytical progress is difficult to make, and we resort to the approximation (36):

$$W_2 = 8\mu \int_0^\infty \frac{dw}{1+w^2} \ln\frac{2wL_0+1}{2wL_0}. \tag{C4}$$

We now minimize $W = W_1 + W_2$ with respect to L_0 and obtain the relation (66) between L_0 and μ. Numerical comparison shows that $\mu(L_0)$ so obtained differs by less than 3% from the result of using the exact kernel Q in Eq. (C3).

[1] C.C. Tsuei, J.R. Kirtley, C.C. Chi, L.S. Yu-Janes, A. Gupta, T. Shaw, J.Z. Sun, and M.B. Ketchen, Phys. Rev. Lett. **73**, 593 (1994).

[2] J.H. Miller, Jr., Q.Y. Ying, Z.G. Zou, N.Q. Fan, J.H. Xu, M.F. Davis, and J.C. Wolfe, Phys. Rev. Lett. **74**, 2347 (1995).

[3] J.R. Kirtley, C.C. Tsuei, M. Rupp, J.Z. Sun, Lock See Yu-Jahnes, A. Gupta, M.B. Ketchen, K.A. Moler, and M. Bhushan, Phys. Rev. Lett. **76**, 1336 (1996).

[4] J. Mannhart, H. Hilgenkamp, B. Mayer, Ch. Gerber, J.R. Kirtley, K.A. Moler, and M. Sigrist, Phys. Rev. Lett. **77**, 2782 (1996).

[5] R.G. Mints and I.B. Snapiro, Phys. Rev. B **49**, 6188 (1994); R.G. Mints and I.B. Snapiro, *ibid.* **51**, 3054 (1995).

[6] J. Pearl, Appl. Phys. Lett. **5**, 65 (1964).

[7] V.G. Kogan, Phys. Rev. B **49**, 15 874 (1994).

[8] *Handbook of Mathematical Functions*, edited by M. Abramowitz and A. Stegun (U.S. GPO, Washington, D.C., 1965).

[9] A. Gurevich, Phys. Rev. B **46**, 3187 (1992).

[10] For grain boundaries in YBCO, l is T independent for large misalignment angles. For small angles, the boundaries behave as superconductor-normal-superconductor junctions, unlike superconductor-insulator-superconductor structures which are discussed in the text. On the other hand, j_c of small angle boundaries might be large, which reduces l and makes the case $l/\Lambda \ll 1$ possible not only near T_c.

[11] I.S. Gradshteyn and I.M. Ryzhik, *Tables of Integrals, Series, and Products* (Academic Press, New York, 1980).

[12] N.N. Bogoliubov, and Y.A. Mitropolsky, *Asymptotic Methods in the Theory of Non-linear Oscillations* (Hindustan Publishing Corp., Delhi, 1961).

[13] A. Seeger, *Teorie der Gitterfehlstellen*, in *Handbuch der Physik* (Springer, Berlin, 1955), Vol. 7, Part 1.